

Structural evolution of nanocrystalline Pd–Mg bilayers under deuterium absorption and desorption cycles

R. Checchetto^{a,*}, R.S. Brusa^a, N. Bazzanella^a, G.P. Karwasz^a, M. Spagolla^a, A. Miotello^a,
P. Mengucci^b, A. Di Cristoforo^b

^aDipartimento di Fisica dell'Università di Trento, I-38050 Povo (TN), Italy

^bDipartimento di Fisica e Ingegneria dei Materiali e del Territorio, Università Politecnica delle Marche, I-60131 Ancona, Italy

Abstract

Grazing incidence X-rays diffraction (GI-XRD), X-rays reflectivity (XRR) and positron annihilation spectroscopy (PAS) analysis on Pd–Mg thin bilayer films deposited by electron-gun on Si wafer and glass substrate evidence a two-region structure: (i) a surface region consisting of the Pd capping layer, the Mg–Pd interface and some Mg subinterface layers; because of the interface roughness, in this region the deposited Mg layers are encased in Pd and, upon the metal to deuteride phase transition, they became highly compressed by the Pd capping layer; (ii) a second region consisting of a pure Mg layer, which extends up to the substrate. This two-region structure is stable upon repeated D₂ absorption and desorption cycles. PAS analysis reveals the formation of vacancy-like defects after D₂ desorption at a concentration higher than that of the as-deposited sample. The two-region structure and the defect dynamics observed in the present study can explain the presence of two peaks in the deuterium desorption spectrum and the diminished D₂ storage efficiency after the first D₂ absorption and desorption cycles.

© 2004 Elsevier B.V. All rights reserved.

Keywords: Pd–Mg bilayers; Absorption cycle; Desorption cycle

1. Introduction

Metal hydrides represent a promising way for hydrogen storage once limitations due to the poor gravimetric efficiency of that having commercial character, such as FeTi and LaNi₅, are overcome [1]. Mg is one of the most studied metal because the hydride presents good gravimetric (~7.6 wt.%) and volumetric efficiencies (~150 kg H₂/m³) and because it forms weaker Mg–H bonds (~126 kJ/mol) than Ca (~168 kJ/mol) and Li (~238 kJ/mol) do [2]. Practical applications of Mg are limited by the slow hydrogen absorption and desorption kinetics due to the surface reactivity and diffusivity of H atoms in the β-MgH₂ phase. The surface reactivity can be enhanced by metallic additives, such as Pd or Nb nanoparticles, dispersed at the

Mg surface [3]. The additive particles act as catalyst for the H₂ molecule dissociation, stimulating the subsequent jumping of the H atoms in the subsurface layers of Mg. Due to the relevance for applications, most of the studies reported in literature on the magnesium–catalyst system are devoted to the search of the optimum catalyst material. Only a limited number is dedicated to the analysis of more fundamental points such as the microscopic processes leading to the catalytic effect and the structural evolution of the magnesium–catalyst interface upon hydrogen absorption and desorption cycles [4]. The relevance of the interface between nanocatalyst and magnesium has been recently suggested by Yavari et al. [5] in the diffraction analysis of catalysed MgH₂ nanocomposites by high-resolution synchrotron radiation: The authors suggested that, after H₂ dissociation at the catalyst surface, the interface acts as a sink for the H atoms, thus representing the path of H atoms into the Mg layers.

In this paper, we present an experimental study based on positron annihilation spectroscopy (PAS) and grazing

* Corresponding author. Tel.: +39 0461 881650; fax: +39 0461 881696.

E-mail address: checchet@science.unitn.it (R. Checchetto).

incidence X-rays diffraction (GI-XRD) on the structural evolution and defects dynamics of Pd-coated Mg thin films upon deuterium absorption and desorption cycles, leading to the formation and dissociation of the deuteride phase (cycling).

2. Experimental details

Mg–Pd bilayers were deposited by electron gun on microscope glass substrates and on (100)-oriented Si by the sequential evaporation of Mg and Pd layers at a grow rate of approximately 0.1 and 0.01 nm/s for Mg and Pd, respectively. A list of the prepared samples is presented in Table 1. During the deposition, the substrate temperature never exceeded 310 K, and the background pressure remained in the low 10^{-6} Pa range (H_2 is thus the dominant contribution of the residual vacuum). Immediately after deposition, the samples were transferred into a treatment chamber pumped to pressure lower than 10^{-4} Pa and, after flushing at room temperature with purified hydrogen, submitted to thermal annealing at 373 K in 99.99% pure D_2 gas at 1.5×10^5 Pa pressure. This procedure stimulates deuterium absorption in Mg and promotes the metal-to-hydride phase transition.

The crystallographic structure of the samples was investigated by an INEL CPS 120 diffractometer in grazing incidence geometry (GID) at 0.4° , 0.8° , 1° and 2° of incidence at 30 kV and 30 mA using the Cu- K_α radiation, whereas a Bruker D8 Advance diffractometer (40 kV, 30 mA, Cu- K_α radiation) was used in total reflection condition [X-rays reflectivity (XRR)] to obtain information on thickness, density and interface roughness of the deposited samples. This information was derived by simulating the XRR curves with the REFSIM program [6]; the maximum experimental error is 3% on the thickness, 10% on the roughness and 5% on the density.

The open volume defect distribution in the samples was depth profiled by PAS [7]. The Doppler broadening of the 511-keV annihilation line due to the electron–positron momenta was measured using a slow positron beam coupled with a high-purity Ge detector (1.2 keV resolution at 511 keV). The shape of the annihilation line was characterized by the S parameter, i.e., the fraction of the positron annihilating with an electron in the low-momentum range

($p_l=0-0.33 \times 10^{-3} m_0c$, where p_l is the electron–positron momentum component in the detector direction). The S parameter was measured as a function of the positron implantation energy in the 0.1–25 keV range; with these energies, a layer from 1 to about 3000 nm can be sampled. The mean positron implantation depth is not linearly related to the positron implantation energy [8]. The statistical uncertainty of the measured S value is of the order of 1×10^{-3} . Energetic implanted positrons in the sample slow down to thermal energies in a few picoseconds; they then diffuse in the material until they annihilate with an electron. However, before being annihilated, they can be efficiently trapped into open volume defects (vacancies, vacancy clusters or voids). Positrons trapped in open volume defects predominantly annihilate with the low momentum electrons of the atoms and contribute to an increase of the S value. Consequently, an increase of the S parameter value, with respect to the S value of a reference sample, is an indication of an increase of the number and/or size of open volume defects. In positron depth profiling measurements, it is difficult to point out directly the contribution that the positron implanted at certain depth gives to the measured S parameter because of the combined effect of the positron implantation profile and of the diffusion process. To extract the S characteristic values of positron annihilating in the different layers, the measured data of samples 1–7 were analysed with the VEPFIT program based on the solution of the stationary diffusion equation in a multilayer structure of different materials [9].

3. Results and discussion

GID spectra of samples consisting on a 15- or 30-nm-thick Pd film on Si substrates, not reported here, indicate the formation of a good crystallized Pd layer growing with the (111) preferred orientation. The analysis of the XRR spectra confirms the thickness of the deposited Pd layers and indicates densities of 13.00 and 11.12 g/cm³, compatible with that of bulk Pd, 12.004 g/cm³. PAS measurements on the same samples show that the defect concentration in the Pd coating is larger near the Pd/Si interface. Samples 1 to 4 produce similar GID spectra and show the nanocrystalline structure of the deposited samples: From the Debye–Scherrer analysis, we evaluate grain dimension in the 20- and 10-nm range for Mg and Pd, respectively. In Fig. 1, we present the GID spectra of sample 1. Spectra reveal a lower crystalline degree of the near-surface Mg layers compared with that of the Mg layers close to the substrate: At 0.4° and 0.8° of incidence, we observe, in fact, larger and less defined Mg peaks compared with that obtained at 1° and 2° . The GID peak at $\sim 35^\circ$ measured at 0.4° incidence, for example, appears very broad and, in sample 1, can be deconvoluted in a peak at $2\theta=34.36^\circ$, pertinent to the Mg (002) reflection and in a less intense peak at $2\theta=35.16^\circ$, which can be attributed to the (300) Mg₅Pd₂ reflection [10].

Table 1
List of prepared Pd–Mg bilayer thin film samples

Samples	Pd layer thickness (nm)	Mg layer thickness (nm)	Substrate
1	15	300	Si
2	30	300	Si
3	15	500	Si
4	30	500	Si
5	15	75	Microscope glass
6	15	150	Microscope glass
7	15	300	Microscope glass

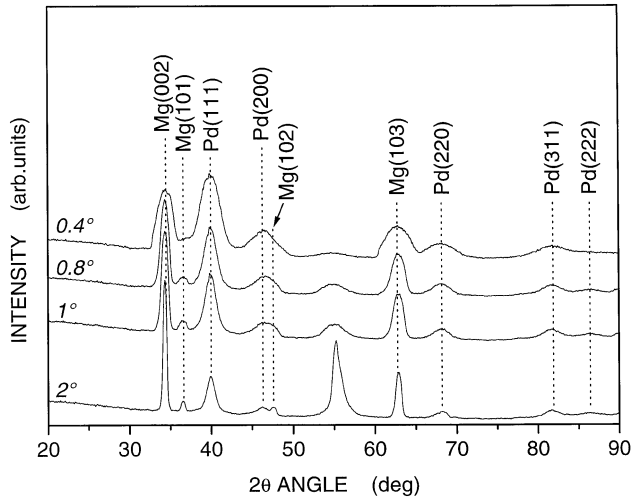


Fig. 1. GI-XRD spectrum of the as-deposited 15 nm Pd–300 nm Mg bilayer film sample.

This second peak shows a remarkable shift with respect to the nominal position $2\theta=34.94^\circ$, indicating an overstoichiometric Pd content. The low crystalline degree of the Mg subinterface layers is likely due to the migration of Pd atoms across the Mg–Pd interface: The formation of Mg–Pd phases at room temperature is in line with the indication of the Mg–Pd phase diagram [11].

The XRR analysis reveals, in samples 1 to 4 and 7, a high interface roughness comparable with the Pd layer thickness. To obtain the best fit of the XRR spectrum of sample 1, not reported here, it was necessary to assume a surface Pd layer with thickness of 12 nm and an effective density of 5.18 g/cm^3 , followed by a second layer 360 nm thick, with an effective density of 2.07 g/cm^3 and interface roughness of $\sim 8 \text{ nm}$. This second layer can be associated with the deposited Mg (1.73 g/cm^3 density). As reported at the beginning of this section, the Pd layer deposited on Si shows a density value equal to that of the bulk material ($12 \pm 1 \text{ g/cm}^3$); the Pd surface layer of sample 1 shows, on the contrary, a much lower effective density. This effective density value of Pd can be explained by the high value of the Mg–Pd interface roughness. Due to the high roughness value, the morphology of this surface region is that of a distribution of Mg clusters encased in a Pd environment. The data on the other samples (2 to 4 and 7) are even more difficult to be fitted due to larger interface roughness than in sample 1. The formation of the Mg–Pd interdiffused region at the interface, see the GID spectrum of the as-deposited sample measured at 0.4° , can also influence the effective value of the surface Pd density: Mg_5Pd_2 has, in fact, a density of 4.18 g/cm^3 , which is comparable with that of the evaluated one. This second effect, however, cannot completely explain the observed results, as the GID spectra clearly show that only a small fraction of the as-deposited Pd atoms forms any Mg–Pd phase. This structure of the interface region appears stable also upon D_2 absorption and desorption cycles: The GI-XRD spectrum of sample 1 after

cycling show a weak peak at $2\theta=31.50^\circ$ due to the (210) reflection peak of the Mg_5Pd_2 phase [10] and crystalline refinement of the h-Mg near interface layers, as shown by a well-defined Mg (002) reflection peak.

The PAS spectra of the deposited and cycled samples 5, 6 and 7 are reported in Fig. 2. The best fit to the experimental PAS spectra of samples 1 to 7 has been obtained by modelling the deposited material as composed of four layers: (i) a thin capping layer of Pd with density $\sim 12 \text{ g/cm}^3$ ($12 \pm 1 \text{ nm}$ in samples 2 and 4; $5 \pm 1 \text{ nm}$ in the other samples); (ii) an extended interface with density $\sim 5 \text{ g/cm}^3$ and thickness 20–50 nm, depending on the thickness of the Mg layer and on the different treatments; (iii) the Mg film with density $\sim 1.7 \text{ g/cm}^3$ up to the nominal thickness; and

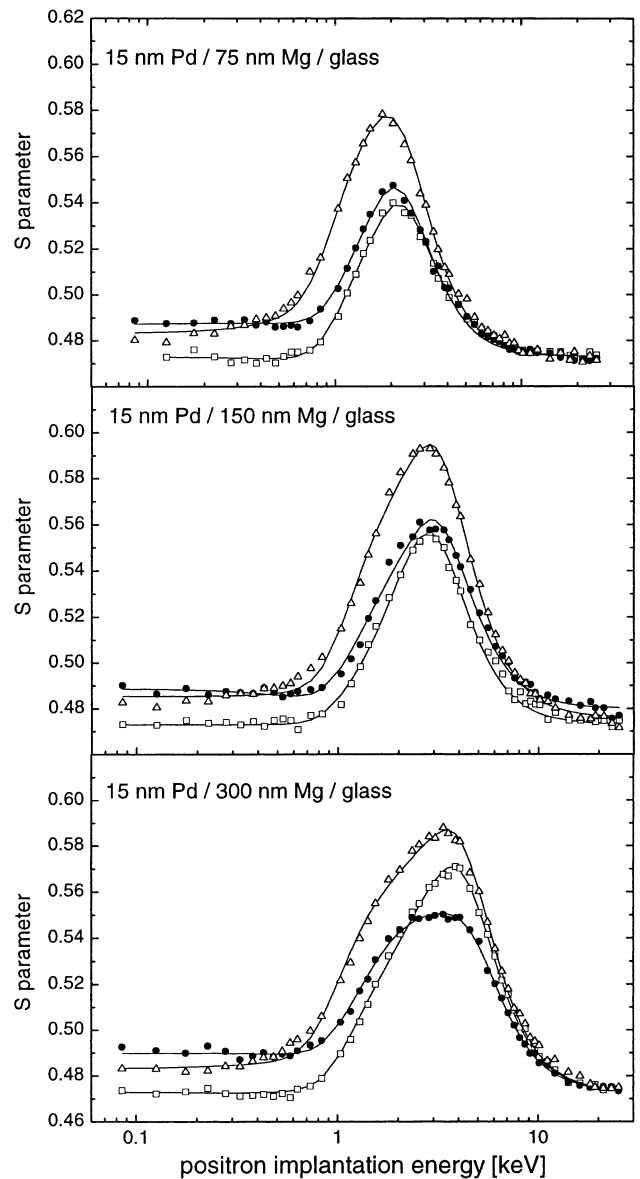


Fig. 2. PAS spectra (S vs. positron implantation energy) of Pd–Mg thin films on glass substrate. ●: As-deposited samples. □: Upon D_2 absorption, leading to the h-Mg to $\beta\text{-MgD}_2$ phase transition. △: Samples after deuterium desorption. The continuous lines are the best fit to the data.

(iv) the glass or the Si substrate. By the fitting procedure, the positron diffusion length was found to be in the 1- to 2-nm order in the three first layers and into the glass substrate (to be compared with 200 nm in Si crystal). This indicates that the Pd and Mg structures are rich of positron trapping sites (vacancy-like defects).

The presence of an unsharp interface, in agreement with the XRR measurements, can be associated to the roughness of the Mg surface and to a possible intermixing of Mg and Pd. The apparent disagreement with the thickness values of the interface, as extracted by XRR curves, is due to the fact that positrons probe the defective structure of an interface layer that can extend more deeply than the estimated roughness. The small increase of the S parameter in the first layer (4–6 nm of Pd up to 1.3 keV in Fig. 2) after deuterium thermal desorption indicates an increase of vacancy-like defects in the Pd capping. The most important result shown by the PAS spectra is the large concentration increase of the vacancy-like defects in the Mg layers and Pd–Mg interface (corresponding to positron implantation energies between 1.3 and 6 keV). The S parameter of the interface appears to be slightly smaller than the S values in the Mg film in all the as-deposited and cycled samples, most probably because of the presence of Pd. The defect concentration in the as-deposited Mg layers increases with the sample thickness (S values in the Mg films, as extracted by the fitting procedure, are equal to 0.592, 0.586 and 0.56 in the 300-, 150- and 75-nm-thick films, respectively); however, after D_2 absorption and desorption cycles, the layers present the same high concentration of vacancy-like defects ($S=0.602\pm 0.012$). The S parameter values in the deuterated Mg layers are lower than those in the as-deposited Mg layers but cannot be directly compared because the samples present different compositions and different crystalline structures (hexagonal Mg vs. distorted tetragonal β -MgD₂).

The structure of the present samples and the observed defect dynamics can explain some peculiarities of the deuterium TDS spectra. In a previous study [12], we observed that the deuterium desorption process was controlled by the decomposition of the Mg deuteride phase. In the film samples with thickness larger or equal to 300 nm, deuterium desorption occurred at temperature of ~ 390 K, which is very low compared with that of the bulk material, $\sim 500\text{--}600$ K [4,13]. The desorption spectra was characterized by the following peculiarities:

- The desorption peak, which presented a shoulder in the low-temperature side, was given by the convolution of a low-temperature peak at $T \sim 370$ K and the dominant peak at ~ 390 K. The low-temperature peak appeared after short thermal treatment times of the sample in D_2 atmosphere, ~ 1 h, then evolved in a broad peak for longer times, and finally, after typical times ~ 10 h, produced the complete desorption spectrum (see Fig. 3 and Ref. [12]).

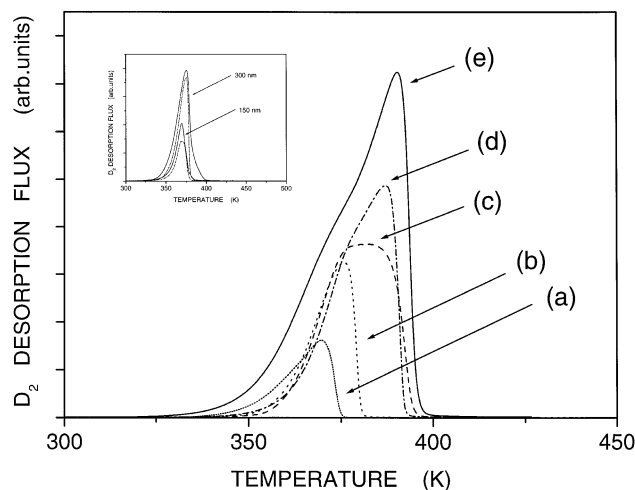


Fig. 3. Evolution of the TDS spectrum of a 15 nm Pd–65 nm h-Mg bilayer sample upon different treatment times in the D_2 atmosphere: (a) short to (e) long times. In the inset, we present the TDS spectra of the 15 nm Pd–150 nm Mg and of the 15 nm Pd–300 nm Mg samples after the first (continuous line) and second (dotted line) deuterations.

- The TDS spectra of the same sample presented differences between the first and second deuteriation showing a lower total integrated area, evidence of a reduction in the deuterium storage capacity of the thin film sample (see inset of Fig. 3 and Ref. [12]).

We suggest that the double peak of the deuterium TDS spectrum of the samples, with an Mg layer larger or equal to 300 nm, is connected to the double-region structure of the present samples. The dominant peak at high temperatures is due to the dissociation of the Mg deuteride phase nucleated in the Mg layers occurring with activation energy of 1.13 ± 0.03 eV, and the shoulder in the low-temperature side of the TDS peak could be explained by the dissociation of the Mg deuteride phase nucleated in the Mg nanograins located at the Mg–Pd interface region occurring with an activation energy of 1.01 ± 0.02 eV [12]. The XRD spectra of the present deuterated samples only show diffraction peaks pertinent to Mg deuteride (see Ref. [12]): The absence of Pd–D or Mg₂–D XRD peaks indicates that deuterium absorbed by the thin Pd surface layer was completely desorbed while exposing the deuterated sample to ambient conditions. We note that the H_2 desorption peak observed by Higuchi et al. [14] at similar temperatures in the TDS spectrum of Pd–Mg bilayers was attributed to the desorption of hydrogen located at the interface boundary between Pd and Mg. It is worthy to report that Cuevas and Hirscher [15], in a study of the hydrogen desorption from Pd films, observed that the TDS spectra consist on a single peak at about 265 K; this temperature is lower than that observed in the present samples.

The lower value of the activation energy clearly indicates a lower stability of the deuteride phase in the surface region, which is probably due to the high level of compressive stresses. These stresses have their origin in the high value of

the roughness of the Mg–Pd interface. Upon the metal-to-deuteride phase transition, there is, in all metals, a volume expansion of the reacting material (the elementary cell can increase its volume by up to 30%). In the surface region of the present samples, as a consequence of the surface roughness, this expansion is strongly limited in the direction parallel to the substrate plane, by the constrain due to the Pd material encasing Mg and, upon deuteration, β -MgD₂. The influence of the elastic stresses in the equilibrium H₂ storage properties of hydride forming materials is well known [16]. In nanocrystalline materials, they have origin in the stress on the nanograins produced by the intragrain regions (grain boundary), which are hydrogenated first, expand and put the nanograins under negative pressure. The consequence is a narrowing of the two-phase region of the phase diagram (miscibility gap) and a lowering of the H₂ gas equilibrium pressure with the hydride. The present analysis assumes that the stresses not only influence the equilibrium properties of the deuterium–magnesium system but also the kinetic of the desorption processes. We cannot exclude that the lower crystalline degree of magnesium in the surface region, as shown by the GI-XRD analysis at 0.4° incidence angle in Fig. 1, can also contribute to a lower stability of the reacted material.

The reduction of the deuterium storage capacity that occurs between the first and second deuteration process [12] is accompanied by an increase of the vacancy-like defect concentration of Mg, observed by PAS spectroscopy (see Fig. 2). This detrimental effect can have a different explanation. The reduction of the storage capacity can be the consequence of kinetic effects related to a reduction of the D atoms diffusivity due to trapping in the observed vacancy-like defects. The typical trapping energy of H in metal vacancies is approximately equal to the surface chemisorption energy, which is in the 0.3 to 0.6 eV range [17]. This energy is of the same order as the activation energy for H diffusion in h-Mg and comparable with the activation energy for H diffusion in β -MgH₂. Anyway, because the deuteration conditions of 373 K and 1.5 MPa D₂ pressure provides sufficient driving force to promote the full-metal-to-deuteride phase transition, this suggestion cannot completely explain the experimental observations.

A second possibility is that the reduction of the D₂ storage capacity ~10% [12] is a consequence of a ~10 at.% reduction of “active” Mg atoms, as consequence of vacancy coalescence processes. These “inactive” Mg atoms are that located at the surface of newly formed interface between the Mg lattice and the internal voids. If this were an explanation, we should expect an internal surface area of a factor 5 to 10 larger than the surface area of the Mg film, depending on the sample thickness. Such an internal surface area should produce observable changes on the sample morphology, e.g., blistering, which are not observed by scanning electron microscopy (SEM).

Discarding the two above processes, we thus suggest that the reduction of the storage capacity can be explained by the

reduced crystalline degree of the Mg lattice connected to the increase of vacancy-like defects. Similar effects have been extensively reported on LaNi₅. Upon the first hydrogenation–dehydrogenation cycle, Pitt et al. [18] reported, by neutron diffraction analysis, the formation of lattice defects that were identified as dislocation by Kim et al. [19], using transmission electron microscopy (TEM) analysis, and vacancies by Shirai et al. [20], using PAS analysis in bulk material. It is worthy to note that the pressure-composition isotherms of hydride forming materials strongly depend on the local atomic configuration [3], even if they have the same atomic composition.

We conclude this discussion by remarking that a contribution of this capacity reduction could also come from a partially atomic mixing in the Pd–Mg interface (see Fig. 1) or to Mg surface oxidation caused by the disruption of the Pd coating during D₂ cycling. Alloying and surface oxidation not only improve the hydrogen absorption and desorption kinetics [21,22] but also reduce the number of Mg layers that take part to the metal to hydride phase transition, thus reducing the D₂ storage capacity. Work is in progress to clarify this point.

4. Conclusions

GID, XRR and PAS analysis on Pd–Mg thin bilayer films deposited by electron gun evidence a two-region structure: (i) a surface region formed by the Pd cap, the Mg–Pd interface and a fraction of the Mg subinterface layers, extending up to 20÷50 nm depth and presenting an effective density value of ~5 g/cm³; as consequence of the high value of the interface roughness, in the surface region, the deposited Mg is encased in the Pd deposited layers; (ii) a second region consisting on pure Mg layers extending up to the substrate and presenting an effective density value of 1.7 g/cm³. This two-region structure is stable upon D₂ absorption and desorption cycles.

PAS analysis reveals the formation of vacancy-like defects after D₂ desorption at a concentration higher to that of the as-deposited sample. The two-region structure and the defect dynamics observed in the present study can explain the presence of a two-peak structure in the TDS spectrum observed in the more thicker Mg samples and the lowered value of the D₂ storage capacity after the first absorption and desorption cycles.

References

- [1] Nature 414 (2001) 332.
- [2] D.R. Lide (Ed.), Handbook of Chemistry and Physics, 71st ed., CRC Press, Boca Raton, FL, 1990–1991, p. 9.
- [3] A. Zaluska, L. Zaluski, J.O. Ström-Olsen, J. Alloys Compd. 288 (1999) 217.
- [4] J.F. Pelletier, J. Huot, M. Sutton, R. Schulz, A.R. Sandy, L.B. Lurio, S.G.J. Mochrie, Phys. Rev., B 63 (2001) 52103.

- [5] A.R. Yavari, J.F.R. de Castro, G. Vaughan, G. Heunen, J. Alloys Compd. 353 (2003) 246.
- [6] Version 2.0, Copyright Brucker ASX, 1999.
- [7] A. Dupasquier, A.P. Mills Jr. (Eds.), *Positron Spectroscopy of Solids*, North Holland, Amsterdam, 1995.
- [8] G.C. Aers, P.A. Marshall, T.C. Leung, R.D. Goldberg, *Appl. Surf. Sci.* 85 (1995) 196.
- [9] A. van Veen, H. Schut, J. de Vries, R.A. Hakvoort, M.R. Ijpma, in: Peter J. Schultz, Guiti R. Massoumi, Peter J. Simpson (Eds.), *AIP Conf. Proc.* 218, *Positron Beams for Solids and Surfaces*, American Institute of Physics, London, Ontario, 1990, p. 171.
- [10] International Center for Diffraction Data: Card Number 22-713.
- [11] Thaddeus B. Massalski (Ed.), *Binary Alloys Phase Diagrams*, vol. 2, American Society for Metals, Metal Park, Ohio, p. 1533.
- [12] R. Checchetto, N. Bazzanella, A. Miotello, R.S. Brusa, A. Zecca, A. Mengucci, *J. Appl. Phys.* 95 (2004) 1989.
- [13] H. Reule, M. Hirscher, A. Weisshardt, H. Kronmuller, *J. Alloys Compd.* 305 (2000) 246.
- [14] K. Higuchi, H. Kajioka, K. Toiyama, H. Fujii, S. Orimo, Y. Kikuchi, *J. Alloys Compd.* 293-295 (1999) 484.
- [15] F. Cuevas, M. Hirscher, *J. Alloys Compd.* 313 (2000) 269.
- [16] P. Tessier, R. Schulz, J.O. Ström-Olsen, *J. Mater. Res.* 13 (1998) 1538.
- [17] S.M. Myers, M.I. Baskes, H.K. Birnbaum, J.W. Corbett, G.G. DeLeo, S.K. Estreicher, E.E. Haller, P. Jena, N.M. Johnson, R. Kirchheim, S.J. Pearton, M.J. Stavola, *Rev. Mod. Phys.* 64 (1992) 559.
- [18] M.P. Pitt, E. MacGray, E.H. Kisi, B.A. Hunter, *J. Alloys Compd.* 293-295 (2000) 118.
- [19] G. Kim, S. Lee, K. Lee, C. Chun, J. Lee, *Acta Metall. Mater.* 43 (1995) 2233.
- [20] Y. Shirai, H. Araki, T. Mori, W. Nakamura, K. Sakaki, *J. Alloys Compd.* 330-332 (2002) 125.
- [21] T.J. Richardson, J.L. Slock, R.D. Armitage, R. Kostecki, B. Farangis, M.D. Rudin, *Appl. Phys. Lett.* 78 (2001) 3047.
- [22] P. Hjort, A. Krozer, B. Kasemo, *J. Alloys Compd.* 237 (1996) 74.